Orbital-Dependent Representation of the Correlation Energy Functional: Properties of Second-Order Kohn–Sham Perturbation Expansion

E. ENGEL, H. JIANG

Center for Scientific Computing, J. W. Goethe-Universität Frankfurt, Max-von-Laue-Strasse 1, D-60438 Frankfurt/Main, Germany

Received 13 April 2006; accepted 9 June 2006
Published online 26 July 2006 in Wiley InterScience (www.interscience.wiley.com).
DOI 10.1002/qua.21174

ABSTRACT: Exchange-correlation energy functionals depending on the Kohn–Sham (KS) orbitals and eigenvalues promise to resolve some of the most pressing deficiencies of the local density and generalized gradient approximations. Such functionals can be derived in first-principles fashion by use of standard many-body techniques, using the KS single-particle Hamiltonian as noninteracting reference Hamiltonian. In this way, one can establish an exact relation for the exchange-correlation functional, which provides several options for the derivation and treatment of approximate functionals. Straightforward expansion in powers of the electron–electron coupling constant gives, to first order, the exact exchange of density functional theory (DFT) and, to second order, the simplest first-principles correlation functional. The properties of this second-order correlation functional are reviewed in detail. It is demonstrated that this functional reproduces both the shell structure in the exact correlation potential and dispersion effects. In response to the variational instability of the functional, observed for the Be atom, a simple and computationally efficient extension is suggested and is shown to be quite accurate for the atomic systems considered so far. © 2006 Wiley Periodicals, Inc. Int J Quantum Chem 106: 3242–3259, 2006

Key words: density functional theory; optimized potential method; orbital-dependent functionals; Kohn–Sham perturbation theory

Correspondence to: E. Engel; e-mail: engel@th.physik.uni-frankfort.de

Contract grant sponsor: Deutsche Forschungsgemeinschaft.
Contract grant number: EN 265/4-1,2.

1. Introduction

The Kohn–Sham (KS) approach of density functional theory (DFT) [1–5] is one of the most widely used tools for electronic structure calculations in quantum chemistry and material science. Present-day applications are usually based on the generalized gradient approximation (GGA) [6–8] for the exchange-correlation (xc) energy functional E_{xc}. Compared with the local density approximation (LDA), the GGA provides much-improved ground-state energies and, at least in most situations, superior equilibrium geometries. However, there are also a number of shortcomings of the LDA that the GGA concept does not resolve; i.e., both approximations (i) fail for the description of atomic negative ions and Rydberg states [9, 10]; (ii) seriously underestimate the bandgap of semiconductors [11]; (iii) often fail to predict the correct ground state if there are several low-lying states that are energetically close (see, e.g., Ref. [12]); (iv) do not reproduce dispersion forces (and often have difficulties with hydrogen bonds); and (v) yield qualitatively incorrect ground states for many strongly correlated solids [13, 14].

To come up with a possible solution to these problems, one has to identify their origin. Problems (i) and (ii) are easily traced back to the incomplete cancellation of self-interaction by LDA and GGA exchange. The self-interaction correction (SIC) component of the true exchange functional has to be as long-ranged as the direct (Hartree) term. The LDA and GGA energy densities and potentials, however, depend on the density $n(\boldsymbol{r})$ in a (semi-)local fashion, i.e., are extremely short-ranged. As a consequence, the LDA and GGA potentials for finite systems asymptotically decay much faster than the exact xc-potential, so that Rydberg states are not bound. In the case of semiconductors, the incomplete SIC leads to a destabilization of the more localized valence band states relative to the conduction band states, resulting in an underestimation of the bandgap. Similarly, problem (iv) is obviously related to the short-range nature of the LDA and GGA correlation functionals. While the role of incomplete SIC and dispersion effects in problems (iii) and (v) is not easily quantified, it is clear that any improvement over the GGA concept has to deal with these two issues.

Once the SIC has been identified as the most important problem to address, it is a natural step to consider use of the exact exchange E_x of DFT [15, 16]. This functional has the same form as the Hartree–Fock (HF) exchange, except that in the Fock (F) term the HF orbitals are replaced by KS orbitals. This idea relies on the fact that the KS orbitals (just as the KS N-particle ground state) are unique functionals of the density by virtue of the Hohenberg–Kohn theorem applied to the noninteracting KS system. The exact E_x is thus an implicit density functional, similar to the KS kinetic energy. Use of the exact exchange immediately resolves all problems related to SIC, ensuring an asymptotically correct xc-potential.

However, for many energetic and structural properties, KS calculations with only the exact exchange (in the following referred to as x-only calculations), i.e., with complete neglect of correlation, give results that are very close to the corresponding HF data [17–22]. The combination of the exact exchange with a conventional density-based correlation functional often leads to less accurate results than pure GGA calculations [23, 24], the reason being the lack of error cancellation between exchange and correlation, which is instrumental for the success of the LDA, but also the GGA. Also, semiempirical orbital-dependent correlation functionals, i.e., the SIC-LDA [25] and the Colle–Salvetti functional [26], have been tested with the exact E_x, but the results, although accurate for some quantities, are generally not satisfactory [27]. Even more important, neither of these correlation functionals is really nonlocal, so that dispersion effects are out of reach anyway.

Fully nonlocal correlation functionals automatically emerge from the application of standard many-body theory, as soon as the KS single-particle Hamiltonian is used as reference Hamiltonian [24, 28–32]. The simplest form of many-body theory is a straightforward perturbation expansion of the xc-energy in powers of the electron–electron coupling constant e^2. The first-order term of this expansion leads to the exact exchange, while all higher-order terms constitute the correlation energy E_c. The lowest-order correlation contribution is thus obtained from second-order perturbation theory. The resulting functional represents the prototype implicit correlation functional, as it is inevitably an important ingredient of all more complete forms. In this contribution, we review the derivation and the properties of this functional, emphasizing both its merits and its limitations. In response to the latter, finally a minimum partial resummation of the perturbation series is put forward.

The present work is organized as follows. Section 2 outlines the general idea of orbital-dependent xc-functionals, the procedure for the calculation of the associated xc-potential, and a Green's function approach to the exact E_c, which then serves as basis for the derivation of the second-order expression for E_c. In Section 3, the latter functional is analyzed in detail, addressing its accuracy for atoms and molecules, its ability to reproduce dispersion forces and its mathematical and variational properties. In Section 4, the particularly simple partial resummation of the perturbation series is introduced and applied to atoms. This study concludes with some final remarks in Section 5. Atomic units are used throughout.

2. Theory

2.1. CONCEPT OF ORBITAL-DEPENDENT FUNCTIONALS

The KS formalism is based on the assumption that for any (nondegenerate) interacting N-electron system with ground-state density $n(\mathbf{r})$, there exists a (nondegenerate) noninteracting N-particle system that has the same ground-state density,

$$\left\{-\frac{\boldsymbol{\nabla}^2}{2}+v_s(\mathbf{r})\right\}\phi_k(\mathbf{r})=\varepsilon_k\phi_k(\mathbf{r}) \tag{1}$$

$$n(\mathbf{r})=\sum_k \Theta_k|\phi_k(\mathbf{r})|^2, \tag{2}$$

where Θ_k characterizes the occupation of the single-particle state k,

$$\Theta_k \equiv \Theta(\varepsilon_F-\varepsilon_k)\equiv\begin{cases}1 & \text{if } \varepsilon_k \le \varepsilon_F\\ 0 & \text{otherwise,}\end{cases} \tag{3}$$

with ε_F denoting the eigenvalue of the highest occupied molecular orbital (HOMO), identified for simplicity with the Fermi energy. As the multiplicative potential v_s of this so-called KS system is uniquely determined by $n(\mathbf{r})$ (by virtue of the Hohenberg–Kohn theorem [1] applied to the noninteracting KS system), all KS single-particle orbitals ϕ_k and eigenvalues ε_k are uniquely determined by the interacting $n(\mathbf{r})$ as well. In the standard KS approach, this fact is used to demonstrate that the KS kinetic energy

$$T_s=-\sum_k \Theta_k \int d^3r\,\phi_k^\dagger(\mathbf{r})\frac{\boldsymbol{\nabla}^2}{2}\phi_k(\mathbf{r}), \tag{4}$$

is a density functional.

However, there is nothing to prevent us from applying this concept as well to the xc-energy functional. In fact, the representation of the xc-functional in terms of ϕ_k and ε_k offers two advantages at the same time. On the one hand, the set of ϕ_k provides much more detailed information on the electronic structure of the KS system than n. In particular, the shell structure of quantum systems is explicitly taken into account by use of the ϕ_k (which is the reason for the dramatic improvement of the KS scheme over purely density-dependent approaches of the Thomas–Fermi type; see, e.g., Ref. [4]). On the other hand, once one allows a ϕ_k dependence of E_{xc}, the derivation of xc-functionals can directly rely on standard many-body methods, which automatically leads to fully nonlocal functionals (in the sense that the xc-energy density and potential at point $\boldsymbol{r}$ do not just depend on $\phi_k(\boldsymbol{r})$ and its first few derivatives, but rather on the form of $\phi_k(\boldsymbol{r}')$ throughout all of space).

The best example for these statements and, at the same time, the most important component of any orbital-dependent E_{xc}, is the exact exchange of DFT,

$$E_x[n]=-\frac{1}{2}\sum_{kl}\Theta_k\Theta_l(kl\|lk), \tag{5}$$

here expressed in terms of the KS-type Slater integral

$$(ij\|kl)=\int d^3r\int d^3r'\,\frac{\phi_i^\dagger(\boldsymbol{r})\phi_k(\boldsymbol{r})\phi_j^\dagger(\boldsymbol{r}')\phi_l(\boldsymbol{r}')}{|\boldsymbol{r}-\boldsymbol{r}'|}. \tag{6}$$

In the case of E_x, the explicit presence of individual quantum states in the functional ensures the exact cancellation of the self-interaction energy, which, by definition, is included in the Hartree energy,

$$E_H[n]=\frac{1}{2}\sum_{kl}\Theta_k\Theta_l(kl\|kl). \tag{7}$$

The exact treatment of the self-interaction energy via (5) automatically resolves several shortcomings of the conventional density functionals. Most notably, it ensures the stability of atomic negative ions

[24, 33], due to the resulting asymptotic $-1/r$-potential [34, 35], and widens the bandgap of semiconductors [36–42], as the attractive SIC affects the valence band states more strongly than the conduction band states. Equation (5) has historically been introduced as a definition [15, 16]. However, as will be shown in Section 2.4, the exchange (5) also emerges from straightforward perturbation theory. Before discussing the derivation of E_x and that of a suitable counterpart for E_c any further, however, the question for the corresponding xc-potential,

$$v_{xc}(\boldsymbol{r}) = \frac{\delta E_{xc}}{\delta n(\mathbf{r})}, \tag{8}$$

has to be addressed.

2.2. OPTIMIZED POTENTIAL METHOD

Let us assume that we have some (yet to be specified) expression for the xc-functional, whose basic ingredients are the KS orbitals and eigenvalues (the derivation and explicit form of such functionals will be discussed in Section 2.3). Of course, such expressions do not allow a direct analytical functional differentiation with respect to $n(\boldsymbol{r})$, as LDA or GGA functionals. Rather, the xc-potential has to be calculated indirectly via solution of an integral equation (or procedures equivalent to that). This optimized potential method (OPM) or optimized effective potential (OEP) can be derived either by minimization of the total DFT energy under the constraint that v_s is a multiplicative potential [34, 43], by the identification of the exact with the KS density [44, 45], or by direct functional differentiation, relying on the chain rule [30] (cf. Ref. [46]). For a general xc-functional of the type $E_{xc}[\phi_k, \varepsilon_k]$, one obtains [31]

$$\int d^3r' \chi_s(\mathbf{r}, \mathbf{r}') v_{xc}(\mathbf{r}') = Q_{xc}(\mathbf{r}). \tag{9}$$

The kernel of this integral equation is given by the static response function of the KS system,

$$\chi_s(\boldsymbol{r}, \boldsymbol{r}') = -\sum_k \Theta_k \phi_k^\dagger(\boldsymbol{r}) G_k(\boldsymbol{r}, \boldsymbol{r}') \phi_k(\boldsymbol{r}') + c.c., \tag{10}$$

with the Green's function $G_k(\mathbf{r}, \mathbf{r}')$ defined as

$$G_k(\boldsymbol{r}, \boldsymbol{r}') = \sum_{l \neq k} \frac{\phi_l(\boldsymbol{r}) \phi_l^\dagger(\boldsymbol{r}')}{\varepsilon_l - \varepsilon_k}. \tag{11}$$

The inhomogeneity of Eq. (9) reads

$$Q_{xc}(\mathbf{r}) = -\sum_k \int d^3r' \left[\phi_k^\dagger(\boldsymbol{r}) G_k(\boldsymbol{r}, \boldsymbol{r}') \frac{\delta E_{xc}}{\delta \phi_k^\dagger(\boldsymbol{r}')} + c.c. \right] + \sum_k |\phi_k(\boldsymbol{r})|^2 \frac{\partial E_{xc}}{\partial \varepsilon_k}. \tag{12}$$

Integration over (9) allows to establish an important sum rule, any E_{xc} has to satisfy (in the case of a completely discrete spectrum),

$$\int d^3r \int d^3r' \chi_s(\mathbf{r}, \mathbf{r}') v_{xc}(\mathbf{r}') = 0 \overset{!}{=} \int d^3r Q_{xc}(\mathbf{r}). \tag{13}$$

Evaluation of the right-hand side of (13) with (12) then leads to [31]:

$$\sum_k \frac{\partial E_{xc}}{\partial \varepsilon_k} = 0. \tag{14}$$

2.3. EXACT XC-FUNCTIONAL FROM KOHN–SHAM MANY-BODY THEORY

Let us now come to actual expressions for $E_{xc}[\phi_k, \varepsilon_k]$. In the first step, an exact relation for E_{xc} will be established, which will subsequently serve as basis for the derivation of approximations. The starting point for the discussion is the noninteracting N-particle KS Hamiltonian:

$$\hat{H}_s = \hat{T} + \int d^3r \hat{n}(\mathbf{r}) v_s(\mathbf{r}), \tag{15}$$

defined by the exact v_s, which is assumed to be known for the moment. The Hamiltonian $\hat{H}$ of the actual interacting system can then be decomposed into $\hat{H}_s$ and a correction $\hat{H}_1$,

$$\hat{H}_1 = \hat{W} - \int d^3r \hat{n}(\mathbf{r}) [v_H(\mathbf{r}) + v_{xc}(\mathbf{r})], \tag{16}$$

where $\hat{W}$ denotes the electron–electron interaction operator, and v_H represents the Hartree potential:

$$v_{\mathrm{H}}(\mathbf{r}) = \int d^3r' \, \frac{n(\mathbf{r}')}{|\mathbf{r} - \mathbf{r}'|}. \tag{17}$$

Applying standard techniques of many-body theory, one can then derive the following exact expression for E_{xc} [31, 46]:

$$E_{\mathrm{xc}} = E_{\mathrm{x}} + \sum_{n=1}^{\infty} \frac{(-i)^n}{(n+1)!} \int_{-\infty}^{\infty} dt_1 \cdots \int_{-\infty}^{\infty} dt_n \times \langle \Phi_0 | T \hat{H}_{1,I}(0) \hat{H}_{1,I}(t_1) \cdots \hat{H}_{1,I}(t_n) | \Phi_0 \rangle_1, \tag{18}$$

where E_{x} is the exchange functional (5), $|\Phi_0\rangle$ is the ground state of the KS system,

$$\hat{H}_{\mathrm{s}} |\Phi_0\rangle = \sum_k \Theta_k \varepsilon_k |\Phi_0\rangle, \tag{19}$$

$\hat{H}_{1,I}(t)$ represents $\hat{H}_1$ in the interaction picture with respect to $\hat{H}_{\mathrm{s}}$,

$$\hat{H}_{1,I}(t) = e^{i\hat{H}_{\mathrm{s}}t} \hat{H}_1 e^{-i\hat{H}_{\mathrm{s}}t}, \tag{20}$$

and T denotes time-ordering [47]. Equation (18) is understood to be evaluated by application of Wick's theorem and the Feynman diagram technique. The index 1 indicates that in this evaluation only diagrams linked to the "external" vertex $\hat{H}_{1,I}(0)$ have to be included. As indicated earlier, the exchange functional (5) emerges automatically from the first-order contribution in $\hat{H}_1$ (which includes additional terms required to end up with the correct DFT total energy). The second term on the right-hand side of Eq. (18) is thus an expression for the exact E_{c}.

Equation (18) represents an exact relation between E_{xc} and the elements of the series of Feynman diagrams on the right-hand side. These elements are the single-particle Green's function of the KS system:

$$G_{\mathrm{s}}(\mathbf{r}, \mathbf{r}', \omega) = \sum_l \left\{ (1 - \Theta_l) \frac{\phi_l(\mathbf{r}) \phi_l^{\dagger}(\mathbf{r}')}{\omega - \varepsilon_l + i\eta} + \Theta_l \frac{\phi_l(\mathbf{r}) \phi_l^{\dagger}(\mathbf{r}')}{\omega - \varepsilon_l - i\eta} \right\}, \tag{21}$$

and the components of the perturbation $\hat{H}_1$, i.e., the Coulomb interaction, v_{H} and v_{xc}. The contributions arising from v_{H} exactly cancel with the so-called tadpole diagrams generated from the Coulomb interaction [31]. One thus ends up with a relation linking E_{xc} with G_{s} and v_{xc}. While the occurrence of G_{s} induces to the desired representation of E_{xc} in terms of ϕ_k and ε_k, the occurrence of $v_{\mathrm{xc}} = \delta E_{\mathrm{xc}} / \delta n$ on the right-hand side of Eq. (18) completely changes the character of this relation: Rather than being an assignment statement, Eq. (18) is a highly nonlinear relation for E_{xc}. Although one can rigorously deal with this nonlinearity in the OPM procedure [31], this feature clearly complicates actual applications. For that reason, in the following, Eq. (18) will only be used for the derivation of approximations that are free of this nonlinearity.

2.4. PERTURBATION EXPANSION: SECOND-ORDER CORRELATION ENERGY

The natural first step of any evaluation of Eq. (18) is a straightforward perturbation expansion in powers of e^2 (KSPT). The formalism then becomes quite similar to the many-body perturbation expansion based on the HF Hamiltonian, usually known as Møller–Plesset (MP) expansion. Nevertheless there are fundamental differences between the MP and KS perturbation expansions. In the MP expansion, due to Brillouin's theorem, the contributions of the single-particle ingredient of $\hat{H}_1$ are exactly cancelled by simple contractions of the two-particle operator in $\hat{H}_1$, which is no longer true in KSPT. As a consequence, KSPT involves additional diagrammatic contributions, absent from the MP expansion. In addition, the spectrum of the KS Hamiltonian is quite different from that of the HF Hamiltonian for the same physical system (due to the asymptotic $-1/r$-decay of the exact DFT exchange potential).

With that in mind let us expand (18) to second order in the coupling constant e^2,

$$E_{\mathrm{xc}} = \sum_{l=1}^{\infty} e^{2l} E_{\mathrm{xc}}^{(l)}[n] = E_{\mathrm{x}} + E_{\mathrm{c}}^{(2)} + \cdots \tag{22}$$

$$v_{\mathrm{xc}} = \sum_{l=1}^{\infty} e^{2l} v_{\mathrm{xc}}^{(l)}[n] = v_{\mathrm{x}} + v_{\mathrm{c}}^{(2)} + \cdots \tag{23}$$

(any $\hat{H}_1$ introduces at least one factor of e^2). Insertion of these expansions into the left- and right-hand side of Eq. (18) yields a well-defined power series in e^2. The second-order term provides the lowest-order correlation contribution. It can be written as the sum of two terms

TABLE I

Correlation energies ($-E_c$, in mHartree) of closed-subshell atoms obtained by insertion of x-only KS orbitals and densities.*

Atom	Exact	VWN	LYP	PBE	E_c^{MP2}	$E_c^{\Delta HF}$	HHEN
He	42	113	44	42	48	0	40
Li	45	152	53	51	49		44
Be	94	225	95	86	124	1	86
N	188	429	192	180	216		186
Ne	391	746	384	351	471	2	420
Na	396	805	408	372	458		419
Mg	438	892	459	411	513	3	457
P	540	1118	566	526	621		560
Ar	722	1431	751	707	846	7	764
MAPE(%)		130	5	6	17		5

* Various correlation functionals in comparison with exact data (taken from Ref. [49]). The HHEN functional is defined by Eq. (58) and discussed in Section 4. The last row provides the mean absolute percentage errors (MAPE) with respect to the exact energies.

$$E_c^{(2)} = E_c^{MP2} + E_c^{\Delta HF}. \quad (24)$$

E_c^{MP2} has the same form as the standard MP2 expression [48]:

$$E_c^{MP2} = \frac{1}{4} \sum_{ijab} \Theta_i \Theta_j \bar{\Theta}_a \bar{\Theta}_b \frac{|(ab\|ij) - (ab\|ji)|^2}{\varepsilon_i + \varepsilon_j - \varepsilon_a - \varepsilon_b}, \quad (25)$$

where $\bar{\Theta}_k \equiv 1 - \Theta_k$. The second term accounts for the fact that the present perturbation expansion is not based on the HF Hamiltonian, but rather on the KS Hamiltonian,

$$E_c^{\Delta HF} = \sum_{ia} \Theta_i \bar{\Theta}_a \frac{|\langle i|\hat{v}_x^{HF} - v_x|a\rangle|^2}{\varepsilon_i - \varepsilon_a}, \quad (26)$$

where

$$\langle i|\hat{v}_x^{HF}|a\rangle = -\sum_j \Theta_j (ij\|ja). \quad (27)$$

The result (24) agrees with that obtained by an equivalent second-order expansion of the adiabatic connection formula for E_c [30].

$E_c^{\Delta HF}$ is well defined as soon as v_x has been determined by solution of the OPM equation (9) for E_x (see Refs. [24, 31]). However, $E_c^{\Delta HF}$ is quantitatively much smaller than E_c^{MP2} and even vanishes for spin-saturated two-electron systems [46] (see also below).

In contrast to the exact E_x, E_c^{MP2} depends on both the occupied and the unoccupied KS orbitals and eigenenergies, which is a common feature of all orbital-dependent correlation functionals obtained from many-body theory on the basis of the KS Hamiltonian. As a result, actual applications are much more demanding than conventional DFT calculations.

3. Analysis of Second-Order Correlation Functional

3.1. ATOMIC CORRELATION ENERGIES

The first step of the analysis of any approximate functional is the perturbative evaluation of the associated energy for some reference systems. The correlation energy is known very accurately for a number of light atoms and some simple diatomic molecules. A comparison of atomic correlation energies is given in Table I, focusing on atoms with spherical spin densities. The latter restriction has the advantage that all quantities required (KS orbitals, densities, gradients, correlation energies) can be calculated on a radial mesh to any desired accuracy, using finite difference techniques. The corresponding results are thus free of any basis set limitations. Table I first of all reflects the fact that atomic E_c are drastically overestimated by the LDA (the VWN form [50] has been applied), while GGAs come rather close to the exact values. This is demon-

TABLE II

Correlation energies ($-E_c$, in mHartree) of closed-subshell atoms.*

	PBE		E_c^{MP2}	
Atom	x-only	Exact	x-only	Exact
He	42	42	48	48
Be	86	86	124	128
Ne	351	350	471	478

* Values obtained by insertion of x-only KS orbitals and densities versus data resulting from exact KS solutions [51].

TABLE III

Energy surface of N_2 at an interatomic separation of 2.07509 Bohr.*

Method	E_b
Expt.	9.91
CCSDTQ	9.905
$E_x + E_c^{(2)}$	14.36

* Exact exchange plus second-order correlation (added perturbatively on basis of x-only calculation) versus CCSDTQ data [52]. Also given is the experimental bond energy [53].

strated for the two most widely used forms, the semi-empirical Lee–Yang–Parr (LYP) GGA [7] and the first-principles Perdew–Burke–Ernzerhof (PBE) GGA [8]. Compared with the GGAs, the average deviation of the second order functional (24) is rather high, independent of whether $E_c^{\Delta HF}$ is included. (Table I explicitly demonstrates the negligible magnitude of $E_c^{\Delta HF}$.) Nevertheless, the improvement over the LDA is quite obvious.

The comparison of Table I is based on densities, orbitals, and eigenvalues obtained from self-consistent calculations with the exact exchange, but without any correlation (x-only calculations). This ensures that in the comparison the corresponding correlation potentials do not play any role, thus focusing completely on the properties of the energy expression (self-consistent results are discussed below). Ideally, this comparison was based on the exact KS orbitals and densities, which are not available, however, for most of the atoms. It is thus worthwhile to remark that the use of the x-only solutions is not completely misleading, as even in the case of orbital-dependent functionals the resulting energies are rather insensitive to the orbitals/densities inserted. This is demonstrated in Table II for a few atoms for which the exact KS solutions are known. Quite generally, both the xc-energies and the xc-potentials of atoms are insensitive to the KS solutions inserted, as long as no self-consistent iteration is involved (compare the result for v_x in Ref. [46]).

In the case of molecules, dissociation energies are generally used for such comparisons, rather than molecular E_c. Table III provides such a comparison for the nitrogen dimer at a bond length of 2.07509 Bohr, with the DFT data based on a self-consistent x-only calculation. Obviously, the overestimation of molecular correlation energies by $E_c^{(2)}$ is even more severe as the deviations observed for atoms.

Unfortunately, Table III does not yet provide the complete picture. If one considers the complete energy surface (E_b) one finds that this functional does not even generate some minimum at all, as shown in Figure 1. With increasing separation of the two atoms $E_c^{(2)}$ becomes increasingly negative, as a result of the shrinking energetic gap between the highest occupied molecular orbital (HOMO) and lowest occupied molecular orbital (LUMO) states (which have Rydberg character in the case of the x-only spectrum). Consequently, the pure second-order KS perturbation expansion can even lead to qualitatively worse results than the LDA or GGA.

3.2. DESCRIPTION OF DISPERSION FORCES

One of the motivations for considering orbital-dependent xc-functionals is the complete failure of the LDA and GGA concepts for the description of dispersion forces. From the functional form of $E_c^{(2)}$

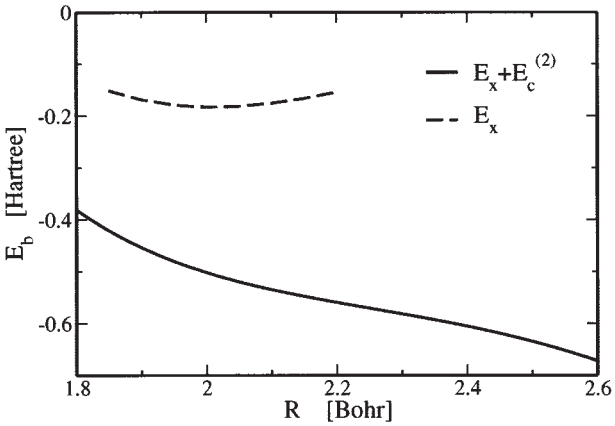

FIGURE 1. Energy surface (E_b) of N_2. Exact exchange plus second-order correlation (added perturbatively on basis of x-only calculations) result versus x-only data.

TABLE IV

van der Waals coefficients C_6 (in atomic units) obtained from Eq. (29) on basis of x-only orbitals and eigenvalues [54].*

Atoms	$E_c^{(2)}$	Empirical
He—He	1.66	1.46
He—Ne	3.49	3.03
Ne—Ne	7.45	6.38
Xe—Xe	730.7	285.9
H—He	3.02	2.82 ± 0.02
H—Na	81.14	71.8 ± 0.3

* Empirical results are taken from Refs. [55, 56].

and its relation to the MP expansion, one would expect this functional to reproduce dispersion forces. A detailed analysis [24, 31] in fact shows that the correlation contribution to the interaction (energy surface) of two well-separated systems A and B resulting from $E_c^{(2)}$ is given by

$$E_{c,\mathrm{int}}^{(2)} = -\frac{C_6}{R^6} \tag{28}$$

$$C_6 = \int_0^\infty \frac{du}{2\pi} \sum_{ijkl=1}^{3} \left(\delta_{ij} - 3\,\frac{R^i R^j}{R^2}\right)\left(\delta_{kl} - 3\,\frac{R^k R^l}{R^2}\right) \times \alpha_{A,ik}(iu)\alpha_{B,jl}(iu), \tag{29}$$

where $\boldsymbol{R}$ is the Cartesian vector connecting A with B and $\alpha_A(iu)$ denotes the atomic or molecular polarizability tensor (evaluated at imaginary frequency),

$$\alpha_{ik}(\omega) = \int d^3r \int d^3r'\, r_i r'_k \chi_s^R(\boldsymbol{r}, \boldsymbol{r}', \omega), \tag{30}$$

whose basic ingredient is the frequency-dependent, retarded KS response function,

$$\chi_s^R(\boldsymbol{r}, \boldsymbol{r}', \omega) = \sum_{i,k} [\Theta_i - \Theta_k] \frac{\phi_i^\dagger(\boldsymbol{r})\phi_k(\boldsymbol{r})\phi_k^\dagger(\boldsymbol{r}')\phi_i(\boldsymbol{r}')}{\omega - \varepsilon_k + \varepsilon_i + i\eta}. \tag{31}$$

Equation (28) has the standard form of the dispersion force. Obviously, $E_c^{(2)}$ is able to reproduce the correct long-range interaction proportional to $1/R^6$. However, the exact result for the coefficient C_6 involves the full atomic polarizabilities, while the present DFT variant of C_6 is determined by the KS polarizabilities (as a consequence of the second-order expansion). A comparison with very accurate C_6 [54] shows that for light atoms Eq. (29) yields reasonably accurate coefficients: Eq. (29) overestimates the full C_6 by 10–20% (see Table IV). In contrast, for heavier atoms higher-order corrections become important, so that Eq. (29) is no longer close to the true result.

It remains to be examined how accurately the second-order functional reproduces the dispersion force if the two systems are less well separated, i.e., for realistic interatomic separations; to predict the equilibrium geometry of a van der Waals bond molecule, it is not just sufficient to have the correct asymptotic $1/R^6$-attraction, but rather the complete energy surface must be accurate. This point is investigated in Figure 2, which shows the energy surface of the He dimer [21]. He_2 is a particularly critical system, as the He_2 bond is extremely weak, leading to a very delocalized ground-state wave function of the nuclei [59]. It thus provides an ideal testing ground for approximate correlation functionals. Figure 2 compares the results from three DFT calculations with HF data [57] and the exact E_b, obtained by variational calculations with correlated wave functions [58] (all E_b are strictly nonrelativistic). Compared with the complete failure of the LDA (the LDA requires the densities of the two atoms to overlap, to produce binding), the second-order functional yields a fairly realistic result. As for atomic E_c and C_6, the agreement with reference results becomes worse with increasing atomic size [21].

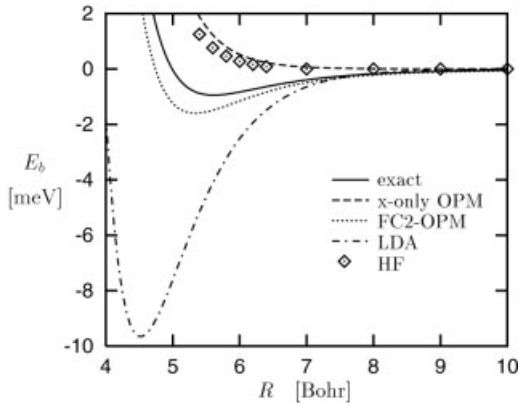

FIGURE 2. Energy surface E_b of He_2. $E_c^{(2)}$ in combination with exact E_x (FC2-OPM) versus LDA, x-only OPM, and HF [57] data, as well as an exact result [58].

3.3. SOLUBILITY OF THE OPM EQUATION

So far, all results discussed were based on a perturbative evaluation of $E_c^{(2)}$. Now the question of the corresponding correlation potential has to be addressed. As discussed in Section 2, its calculation requires the solution of Eq. (9), which is straightforward, although computationally demanding, in the case of the exact E_x. It becomes even more demanding as soon as the complete KS spectrum enters is present in E_{xc} and, in particular, if the inhomogeneity depends on v_x via (26). While the functional derivatives of v_x with respect to the ϕ_k and ε_k can be handled rigorously [31], the resulting computational cost is excessive. Given the negligible magnitude of $E_c^{\Delta HF}$, this part of $E_c^{(2)}$ is therefore dropped in the following. Note that all results are nevertheless exact for spin-saturated two-electron systems, as $E_c^{\Delta HF}$ vanishes identically for these systems.

As they stand, Eqs. (9)–(12) apply to systems with a completely discrete spectrum. For atoms and molecules, such a spectrum is obtained as soon as a basis set is used for the representation of the KS states or suitable boundary conditions are applied (e.g., enclosing the system in a box and requiring hard-wall boundary conditions). In reality, however, free atoms and molecules have a continuous energy spectrum of positive energies, in addition to the occupied levels and the Rydberg-type unoccupied states. Both the orbital-dependent xc-functional itself and the OPM equations have to account for the continuous contribution. Restricting the discussion to closed-subshell atoms, one finds for E_c^{MP2} [60, 61]:

$$E_c^{MP2} = E_c^{DD} + 2E_c^{DC} + E_c^{CC} \tag{32}$$

$$E_c^{DD} = \sum_{\substack{n_1 n_2 n_3 n_4 \\ l_1 l_2 l_3 l_4}} \frac{N(n_1 l_1, n_2 l_2 | n_3 l_3, n_4 l_4)}{\varepsilon_{n_1 l_1} + \varepsilon_{n_2 l_2} - \varepsilon_{n_3 l_3} - \varepsilon_{n_4 l_4}} \tag{33}$$

$$E_c^{DC} = \sum_{\substack{n_1 n_2 n_3 \\ l_1 l_2 l_3}} \int_0^\infty dk \, \frac{N(n_1 l_1, n_2 l_2 | n_3 l_3, \overline{kl})}{\varepsilon_{n_1 l_1} + \varepsilon_{n_2 l_2} - \varepsilon_{n_3 l_3} - \varepsilon} \tag{34}$$

$$E_c^{CC} = \sum_{\substack{n_1 n_2 \\ l_1 l_2 l l'}} \int_0^\infty dk \int_0^\infty dk' \, \frac{N(n_1 l_1, n_2 l_2 | \overline{kl}, \overline{k'l'})}{\varepsilon_{n_1 l_1} + \varepsilon_{n_2 l_2} - \varepsilon - \varepsilon'}. \tag{35}$$

In Eqs. (33)–(35), N abbreviates the appropriate product of occupation factors, angular momentum coupling coefficients, and radial Slater integrals:

$$N(12|34) = \Theta_1 \Theta_2 \bar{\Theta}_3 \bar{\Theta}_4 \times [D(12|34) - X(12|34)] \tag{36}$$

$$D(12|34) = 2 \sum_{L=0}^{\infty} (12|34)_L^2 (l_1 0 l_3 0 | L0)^2 (l_2 0 l_4 0 | L0)^2 \times \frac{(2l_1+1)(2l_2+1)(2l_3+1)(2l_4+1)}{(2L+1)^3} \tag{37}$$

$$X(12|34) = \sum_{L,L'=0}^{\infty} (-1)^{l_1+l_2+l_3+l_4+L+L'} \times (12|34)_L (12|43)_{L'} W(l_1 l_3 l_4 l_2; LL') \times (l_1 0 l_3 0 | L0) \times (l_2 0 l_4 0 | L0) \times (l_1 0 l_4 0 | L'0)(l_2 0 l_3 0 | L'0) \times \frac{(2l_1+1)(2l_2+1)(2l_3+1)(2l_4+1)}{(2L+1)(2L'+1)}, \tag{38}$$

where $(l_1 m_1 l_2 m_2 | LM)$ denotes a Clebsch–Gordan coefficient, $W(l_1 l_3 l_4 l_2; LL')$ a Racah coefficient (both in the definition of Rose [62]) and the radial Slater integral is given by

$$(12|34)_L = \int_0^\infty dr \int_0^\infty dr' \, \frac{r_<^L}{r_>^{L+1}} P_1(r) P_3(r) P_2(r') P_4(r'). \tag{39}$$

Here P denotes a solution of the radial KS equation for either a discrete (ε_{nl}) or a continuous energy $\varepsilon = k^2/2$,

$$\left\{ \frac{-1}{2} \left[\frac{\partial^2}{\partial r^2} - \frac{l(l+1)}{r^2} \right] + v_s(r) - \varepsilon_{nl} \right\} P_{nl}(r) = 0 \tag{40}$$

$$\left\{ \frac{-1}{2} \left[\frac{\partial^2}{\partial r^2} - \frac{l(l+1)}{r^2} \right] + v_s(r) - \frac{k^2}{2} \right\} \bar{P}_{kl}(r) = 0, \tag{41}$$

with the normalization of $\bar{P}_{kl}$ chosen in the standard fashion (cf. Ref. [63]):

$$\bar{P}_{kl}(r \to \infty) \sim \sqrt{\frac{2}{\pi}} \sin\left[kr + \frac{Zm}{k} \ln(2kr) - \frac{\pi}{2} l - \eta_{kl} \right]. \tag{42}$$

In the case of the radial OPM equation,

$$\int_0^\infty dr' K(r, r') v_{xc}(r') = Q_{xc}(r), \tag{43}$$

the continuous spectrum shows up in the radial response function

$$K(r, r') = -4 \sum_{nl} \Theta_{nl}(2l+1) P_{nl}(r) G_{nl}(r, r') P_{nl}(r'), \tag{44}$$

via the radial Green's function,

$$G_{nl}(r, r') = \sum_{n' \neq n} \frac{P_{n'l}(r) P_{n'l}(r')}{\varepsilon_{n'l} - \varepsilon_{nl}} + \int_0^\infty dk \frac{\bar{P}_{kl}(r) \bar{P}_{kl}(r')}{\varepsilon - \varepsilon_{nl}}, \tag{45}$$

and in the inhomogeneity,

$$Q_{xc}(r) = Q^a_{xc,-}(r) + Q^a_{xc,+}(r) + Q^b_c(r) \tag{46}$$

$$Q^a_{xc,-}(r) = -\sum_{nl} \int_0^\infty dr' P_{nl}(r) G_{nl}(r, r') \frac{\delta E_{xc}}{\delta P_{nl}(r')} \tag{47}$$

$$Q^a_{xc,+}(r) = -\sum_{l} \int_0^\infty dk \int_0^\infty dr' \times \bar{P}_{kl}(r) G_{kl}(r, r') \frac{\delta E_{xc}}{\delta \bar{P}_{kl}(r')} \tag{48}$$

$$Q^b_c(r) = \sum_{nl} P_{nl}(r)^2 \frac{\partial E_{xc}}{\partial \varepsilon_{nl}} \tag{49}$$

$$G_{kl}(r, r') = \sum_{n'} \frac{P_{n'l}(r) P_{n'l}(r')}{\varepsilon_{n'l} - \varepsilon} + \mathcal{P} \int_0^\infty dk' \frac{\bar{P}_{k'l}(r) \bar{P}_{k'l}(r')}{\varepsilon' - \varepsilon}. \tag{50}$$

By careful analysis of Eqs. (43)–(45), one can show for both a completely discrete system and the actual spectrum of free atoms [61, 64] that

$$\frac{\int_0^\infty dr' K(r, r') v_c(r')}{\int_0^\infty dr' K(r, r') v_x(r')} \xrightarrow{r \to \infty} \text{const}, \tag{51}$$

as long as

$$\lim_{r \to \infty} v_c(r) = 0. \tag{52}$$

However, in view of (43), Eq. (51) implies

$$\frac{Q_c(r)}{Q_x(r)} \xrightarrow{r \to \infty} \text{const}. \tag{53}$$

Unexpectedly, it turns out that the ratio Q_c/Q_x does not approach a constant in the case of the MP2 energy expression [61, 64, 65]. One concludes that the radial OPM equation (43) for E_c^{MP2} does not have a solution with the standard boundary condition (52).

One can also arrive at this surprising result from a somewhat different perspective. As long as (43) is valid, i.e., as long as the radial OPM equation has a solution, the sum rules (13) and (14) remain valid for spherically symmetric systems:

$$\int_0^\infty dr Q_c(r) = 0 \tag{54}$$

$$\sum_k \frac{\partial E_c}{\partial \varepsilon_k} = 0, \tag{55}$$

where the compliance of the exact E_x with (13) and (14) has been used. Note that the sum in (55) only comprises the discrete states, just as in (49). This is a consequence of the fact that one finds a solution of the KS equation for arbitrary positive energy ε, irrespective of the form of v_s, as long as (52) is satisfied. However, insertion of Eqs. (32)–(35) into (55) immediately shows that (55) is violated in the case of the MP2 functional [61, 65]. Thus, one ends up with the conclusion that the OPM equation for E_c^{MP2} cannot be solved as soon as positive energy continuum states are present.

As already indicated, a completely discrete spectrum can be ensured by hard-wall boundary conditions, which in the case of spherical atoms are imposed by requiring $P_{nl}(r \geq R_0) = 0$ for some (large) radius R_0. This technique can serve both as a mathematical tool for the analysis of the OPM procedure and as a practical technique for performing self-consistent calculations. In the former case, R_0 can be taken arbitrarily large, allowing study of the

transition from a discrete to a continuous spectrum. In this way, one finds [61]

$$\int_0^\infty dr \lim_{R_0\to\infty} Q_c^b(r) \neq \lim_{R_0\to\infty} \int_0^{R_0} dr Q_c^b(r) = 0, \quad (56)$$

which identifies the violation of the sum rule as an order of limits ambiguity. Equation (56) implies that the OPM equation cannot be solved after the continuum limit has been taken for its ingredients.

In contrast, if one keeps R_0 just large enough that the chemical properties of the atom (i.e., the highest occupied and lowest unoccupied states) remain unaffected, one ends up with a practical scheme for application of E_c^{MP2} [66]. In this scheme, each cycle of a self-consistent calculation for a free atom consists of the following steps:

1. For given total potential v_s, solve the radial KS equations for $0 \leq r < \infty$ and construct a new Hartree and exchange potential from the solutions. In practice, this amounts to solving the radial equations on a grid that extends sufficiently far out that all occupied orbitals have vanished. For the large values of R_0 chosen, this is the case before R_0 is reached, so that the solution inside the spherical cavity coincides with the standard procedure for free atoms.
2. For the same total potential v_s, solve the radial KS equations for $0 \leq r \leq R_0$ with boundary condition $P_{nl}(r \geq R_0) = 0$ for the complete spectrum (i.e., for as many positive energy states as one can afford).
3. Construct the Green's function (11), kernel (10), and inhomogeneity (12) for E_c^{MP2} from the solutions and solve (43) in discretized form on the radial mesh (for $0 \leq r \leq R_0$).
4. Extend the resulting v_c^{MP2} into the region $r > R_0$ by adjusting the parameters of the exact asymptotic form of v_c to the numerical data for v_c^{MP2} in the semi-asymptotic region 4 Bohr $< r \ll R_0$, in which the potential of the atom in the cavity is neither affected by a nonvanishing electron density nor by the hard-wall boundary condition at R_0.
5. Add the resulting v_c^{MP2} for the complete space to v_H and v_x to form a new total v_s.

The details of this procedure and a critical assessment of its accuracy can be found in Ref. [66]. All subsequent numerical results for v_c^{MP2} have been obtained with the same technique and parameters as used in Ref. [66]. In particular, a cavity radius of $R_0 = 20$ Bohr has been used, and states up to an energy of $\varepsilon_{max} \sim 1100$ Hartree and an angular momentum of $l_{max} = 6$ have been included in all sums over positive energy states.

As a final remark on the solubility of the OPM equation for E_c^{MP2}, it should be emphasized once more that the use of basis set expansions for both the KS states and the xc-potential also resolves the ambiguity originating from the positive energy continuum [67–69]. However, due to the very different spatial form of orbitals and xc-potentials, this approach requires a very careful treatment of the basis set representation of v_{xc}, in particular in the asymptotic regime. To provide reference results a fully numerical scheme relying on finite differences methods (as the one described above) is clearly advantageous.

3.4. CORRELATION POTENTIAL

3.4.1. Comparison With Reference Data

As the only component of the total KS potential that has to be approximated, the xc-potential is the most critical ingredient of any self-consistent KS calculation. The accuracy of v_{xc}, especially its behavior in the asymptotic region, is particularly important for the quality of the eigenenergies and orbitals. These latter quantities not only are relevant for ground-state properties, but also serve as input to time-dependent DFT (TDDFT) calculations within the linear-response regime.

The asymptotic behavior of the exact v_{xc} is dominated by the exchange potential with its $-1/r-$ decay. Using the exact exchange, one can thus obtain KS spectra that are much more accurate than their LDA/GGA counterparts. However, it is well known that the variation of atomic ionization potentials and, in particular, electron affinities over the Periodic Table can only be reproduced by inclusion of an accurate correlation potential [70]. Moreover, as a microscopic local quantity, the correlation potential is much more characteristic of the performance of an approximate correlation functional than the corresponding energy, similar to the situation for E_x [71].

As the first step of the analysis of the correlation potential corresponding to E_c^{MP2}, a comparison with exact reference data seems most appropriate. Figure 3 compares v_c^{MP2} with the exact v_c of Be and Ne

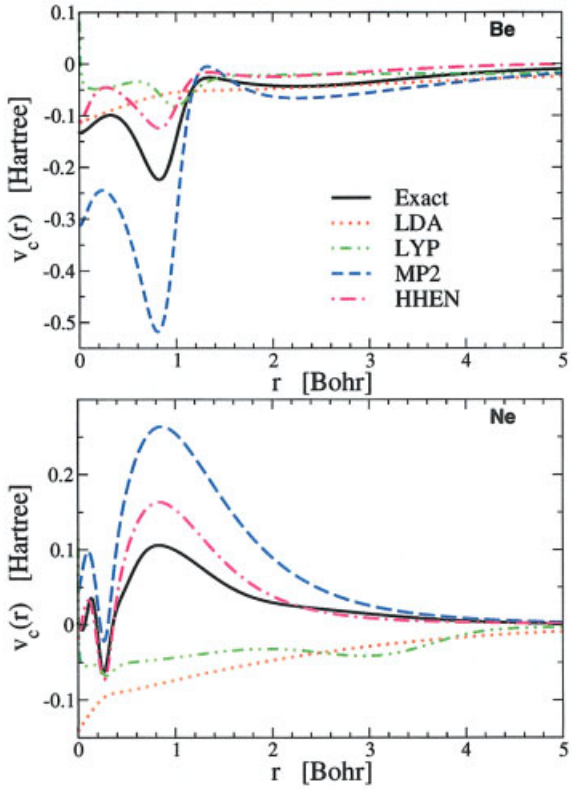

FIGURE 3. Correlation potentials corresponding to the exact ground-state densities of Be and Ne: MP2 (long dash), HHEN (dash-dot), VWN-LDA (dot), and LYP-GGA (dot-dot-dash) versus exact correlation potential (solid) [51]. [Color figure can be viewed in the online issue, which is available at www.interscience.wiley.com.]

[66]. The latter potentials have been obtained by inversion of the radial KS equation for given, highly accurate Monte Carlo densities [51]. Accordingly, v_c^{MP2} is constructed from the orbitals and eigenenergies resulting from the exact KS potentials for these systems. Figure 3 clearly shows that v_c^{MP2} reproduces the shell structure of the exact v_c, including the fact that the correct v_c has to be asymptotically attractive on the left-hand side of the Periodic Table (Be), but repulsive on the right-hand side (Ne). Although the amplitudes of all shell features are by far overestimated by v_c^{MP2}, the improvement over the LDA [50] and the GGA [7] is dramatic.

Figure 4 shows v_c^{MP2} for Li and N. As no exact KS potentials for these spin-polarized atoms are available, the results displayed in Figure 4 are based on the solutions of self-consistent x-only calculations with the exact exchange. Besides the structures already observed for unpolarized atoms, two new features are remarkable when comparing LDA/GGA and MP2 potentials. First, in the core region, in which the electron densities of the two spin channels are essentially identical, $v_{c\uparrow}$ and $v_{c\downarrow}$ are very close in the case of the LDA and GGA. In contrast, $v_{c\uparrow}$ and $v_{c\downarrow}$ differ by an almost constant shift in the case of E_c^{MP2}, which is reminiscent of the derivative discontinuity of the exact E_c. Second, for Li, the MP2 correlation potential of the majority-spin channel, $v_{c\uparrow}$, is mainly attractive, while the minority-spin potential, $v_{c\downarrow}$, is repulsive. In the case of N, the sign of the majority-spin channel is repulsive, while the minority-spin potential remains close to zero in the valence regime and becomes attractive in the core region. This reflects the fact that for Li the majority-spin channel is dominated by the valence 2*s* orbital associated with the left-hand side of the Periodic Table, while the minority-spin channel is determined by the 1*s* state corresponding to the closed-shell He configuration,

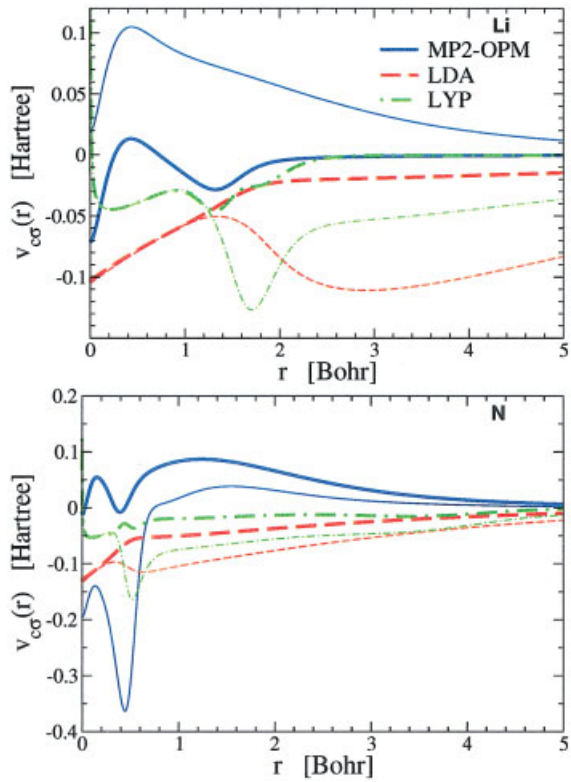

FIGURE 4. Spin-up (thick lines) and spin-down (thin lines) correlation potentials of Li (top) and N (bottom) based on self-consistent x-only densities: MP2 (solid) versus VWN-LDA (dash) and LYP-GGA (dash-dot). [Color figure can be viewed in the online issue, which is available at www.interscience.wiley.com.]

and thus the right-hand side of the Periodic Table. For N with its filled majority-spin 2*p* orbital and its completely unoccupied minority-spin 2*p* orbital, the situation is essentially reversed. This feature, which was also observed for the correlation potentials obtained by inversion of CI spin-densities [72], is completely absent in the case of LDA and GGA potentials.

Taking Figures 3 and 4 together, the first-principles nature of E_c^{MP2} is quite obvious. In contrast, the overestimation of the various structures in the exact v_c is substantial. In fact, the differences between v_c^{MP2} and the exact v_c are larger than those between the latter potentials and $v_c = 0$, reflecting the perturbative nature of E_c^{MP2}.

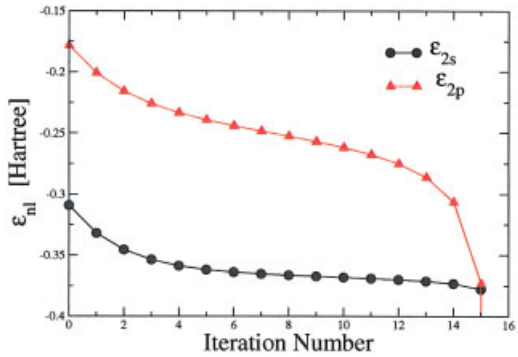

FIGURE 5. Evolution of the HOMO–LUMO gap during self-consistent FMP2–OPM iteration for Be. [Color figure can be viewed in the online issue, which is available at www.interscience.wiley.com.]

3.4.2. Variational Instability

The next step of the analysis of E_c^{MP2} is its self-consistent application. Self-consistent calculations, however, are intrinsically linked to the variational stability of a functional. As an inspection of (25) immediately shows, E_c^{MP2} is unbounded from below; i.e., it approaches $-\infty$ if the energetic gap between HOMO and LUMO states shrinks to zero. Thus, systems for which HOMO and LUMO states are degenerate, like metals, are clearly beyond the regime of applicability. However, the question is whether E_c^{MP2} is variationally stable for systems that, in principle, should have a finite gap. Naively, one expects an unconstrained variational minimization of a total energy functional including E_c^{MP2} to fail due to the unboundedness of E_c^{MP2}. However, E_c^{MP2} is only a minor component of the total energy and v_c^{MP2} is usually small compared with v_{ext}, v_H and v_x. It is thus not clear a priori whether v_c^{MP2} can induce a breakdown of the HOMO–LUMO gap. For instance, in the case of the noble gas elements the energetic separation and the associated spatial separation of HOMO and LUMO states are so substantial that a non-Coulombic potential as v_c^{MP2} should not alter the situation. In contrast, for the alkaline earth elements the HOMO and LUMO states are energetically and spatially close together, so that a minor modification of v_s may lead to degeneracy. Under these circumstances, only actual calculations can clarify the situation.

Self-consistent calculations with the combination of the exact E_x and E_c^{MP2} (denoted by FMP2 in the following) for all closed-(spin-)subshell atoms up to Argon turned out to be convergent, with the only exception of Be [66]. The variational instability observed for the Be atom is easily traced to the closing of the HOMO–LUMO. This is illustrated in Figure 5, which shows the gap during the course of the self-consistent iteration. The instability shows up no matter which initial guess is used for the self-consistent iteration, indicating that it is an intrinsic property of E_c^{MP2}. Although the instability was not observed for Mg, it is to be expected that many similar cases exist.

As a final remark on v_c^{MP2} we note that for all atoms for which the FMP2 iteration is stable the self-consistent v_c^{MP2} shows more pronounced shell oscillations than those calculated perturbatively from either x-only or exact densities.

3.4.3. Self-Consistent Total Energies and Ionization Potentials

The total ground-state energies and HOMO eigenvalues resulting from these self-consistent calculations are listed in Tables V and VI, together with the corresponding LDA and GGA data.

The results obtained with the xc-functionals are compared with the exact values obtained from the combination of experimental ionization energies with highly accurate variational calculations for two- and three-electron systems, corrected for relativistic and recoil effects [49]. Table V demonstrates that the exact exchange plus MP2 correlation gives ground-state energies that are somewhat more accurate than the first-principles PBE-GGA, but somewhat less accurate than the semi-empirical BLYP-functional, in spite of the obvious improvement of v_c.

The latter property becomes more important for the ionization potential (IP), which, on the exact level, is identical with the eigenvalue of the

TABLE V

Absolute total ground-state energies (in Hartree) of spherical atoms obtained by self-consistent calculations: $E_x + E_c^{MP2}$ (FMP2) versus LDA [50], BLYP-GGA [6, 7], PBE-GGA [8], and exact data [49].*

Atom	Exact	LDA	BLYP	PBE	FMP2	FHHEN
He	2.904	2.835	2.907	2.893	2.910	2.901
Li	7.478	7.344	7.483	7.462	7.482	7.476
Be	14.667	14.447	14.662	14.630	14.696[a]	14.659
N	54.589	54.137	54.593	54.536	54.622	54.590
Ne	128.938	128.233	128.973	128.866	129.026	128.969
Na	162.257	161.448	162.293	162.173	162.319	162.278
Mg	200.053	199.139	200.093	199.955	200.129	200.071
P	341.259	340.006	341.278	341.116	341.338	341.276
Ar	527.540	525.946	527.551	527.346	527.661	527.578
$\overline{\lvert\Delta\rvert}$		0.683	0.018	0.079	0.055	0.015
$\lvert\Delta\rvert_{max}$		1.594	0.040	0.194	0.121	0.038

* The energies resulting from the combination of the exact E_x with the partially resummed functional (58) (FHHEN) are also listed. The last two rows show the mean and maximum absolute errors, respectively, with respect to the exact energies [49].
[a] From perturbative calculation based on the x-only density.

HOMO KS state [73]. The difference between the exact IP and the HOMO eigenenergy therefore provides a simple quantitative measure of the accuracy of the xc-potential. Table VI illustrates the well-known fact that LDA and GGA yield poor results, with the GGA not improving over the LDA. The combination of the exact exchange with the LYP-GGA (FLYP), though much more accurate than pure LDA or GGA data, gives less accurate results than x-only calculations. This again demonstrates the complete failure of GGAs to reproduce atomic v_c. The FMP2-functional also does not improve over the *x*-only results. This, at first glance, surprising result originates from the drastic overestimation of the shell oscillations by v_c^{MP2}: The overestimation leads to a correlation potential which is further away from the exact v_c than the trivial approximation $v_c = 0$.

TABLE VI

HOMO eigenvalues (in mHartree) of spherical atoms obtained by self-consistent calculations: $E_x + E_c^{MP2}$ (FMP2) versus x-only (F), LDA [50], BLYP-GGA [6, 7], PBE-GGA [8], exact E_x plus LYP correlation (FLYP), and exact data [49].*

Atom	Exact	F	LDA	BLYP	PBE	FLYP	FMP2	FHHEN
He	903	918	570	585	579	950	893	915
Li	198	196	116	111	119	200	198	198
Be	343	309	206	201	206	330	—	324
N	534	571	309	297	307	585	499	533
Ne	792	851	498	491	491	890	656	763
Na	189	182	113	106	113	189	191	189
Mg	281	253	175	168	173	274	305	273
P	385	392	231	219	233	403	385	386
Ar	579	591	382	373	378	624	557	576
$\overline{\lvert\Delta\rvert}$		22	178	184	178	31	28	8
$\lvert\Delta\rvert_{max}$		59	333	318	324	98	136	29

* The energies resulting from the combination of the exact E_x with the partially resummed functional (58) (FHHEN) are also listed. The last two rows show the mean and maximum absolute errors, respectively, with respect to the exact ionization potentials [49].

Taking the results of Sections 3.3 and 3.4 together, it is clear that E_c^{MP2} can only be considered a first step. Higher-order correlation contributions have to be included to arrive at qualitatively and quantitatively satisfying results. However, before addressing this aspect further, some remarks on the nonlocality of v_c^{MP2} seem to be in order.

3.5. QUASI-LOCALITY OF CORRELATION POTENTIAL

In conventional correlated ab initio calculations for systems involving heavier atoms virtual excitations of the atomic core states are usually neglected. The same is automatically true for corresponding pseudo-potential calculations. As in the core region, the total potential is dominated by the nuclear potential and the Hartree potential remains close to its atomic form, core orbitals are rather inert to a change of the chemical environment. As a consequence, their contribution to the correlation energy cancels out in the energy surface. However, the accurate treatment of particle-hole excitations of core electrons requires virtual states of very high energy. Neglect of core excitations therefore greatly reduces the computational demands without sacrificing accuracy.

In the case of orbital-dependent correlation functionals a similar treatment is desirable. However, in the context of DFT, the procedure for calculating the correlation potential, i.e., the OPM integral equation, introduces an additional coupling between the core and the valence region, which differs from the coupling originating from the intrinsic nonlocality of first-principles functionals like E_c^{MP2}. It is thus not clear a priori whether the neglect of virtual core excitations in the functional leaves the correlation potential in the valence region invariant.

Figure 6 shows the MP2 correlation potentials of Zn and Cu obtained by inclusion of differently many core states in E_c^{MP2}: The complete v_c^{MP2} is compared with the potentials that result from the expression (25) with selected core states dropped from the sums over i and j. All other ingredients of the OPM procedure are left unchanged, in particular the Green's function (11). The OPM equation is solved for given x-only orbitals and eigenvalues. Figure 6 demonstrates that the neglect of a particular core shell leads to a modification of v_c^{MP2} only in that region in which this shell is localized. In spite of the nonlocality of the OPM the final contribution of a given shell is rather local. This quasi-locality of the OPM justifies the neglect of core

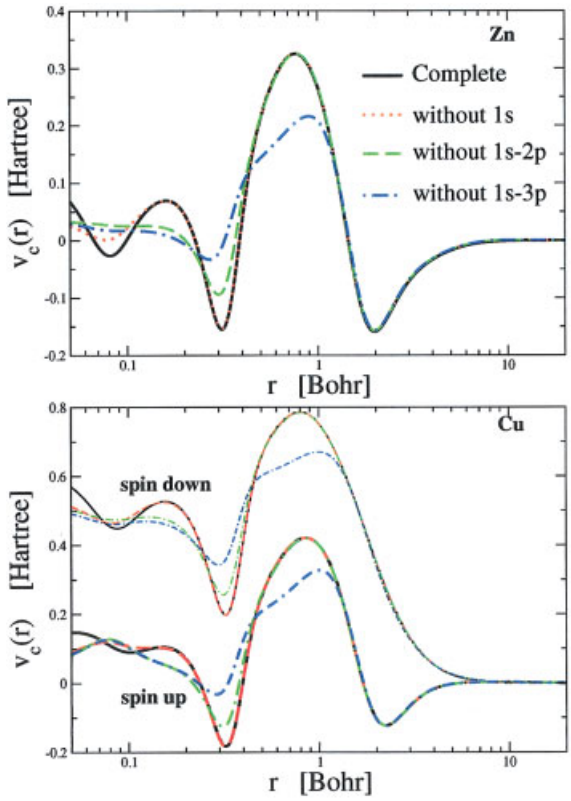

FIGURE 6. MP2 correlation potential of Zn and Cu obtained by including differently many core states in E_c^{MP2}, when calculating the OPM inhomogeneity (12). [Color figure can be viewed in the online issue, which is available at www.interscience.wiley.com.]

excitations in the framework of orbital-dependent xc-functionals.

However, Figure 6 also shows that this neglect has to be consistent in the sense that one should not break up shells: If the 3*s* and 3*p* states are dropped, while the 3*d* orbital is kept in (25), the resulting potential no longer agrees with the complete v_c^{MP2} in the region of the M-shell. The intra-shell overlap is much too high to be neglected without affecting v_c^{MP2}. Consequently, only complete shells should be dropped. It seems worthwhile to remark that the same is true for the exact exchange.

4. Higher-Order Correlation Via Partial Resummation

As is clear from the results discussed in Section 3, the inclusion of higher-order correlation is mandatory in order to resolve several shortcomings of

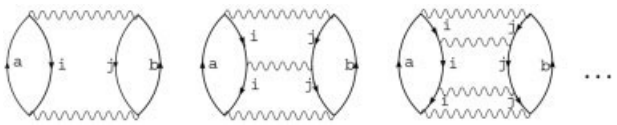

FIGURE 7. Diagrammatic representation of the hole–hole Epstein–Nesbet perturbation series, E_c^{HHEN}, in which the diagonal contributions to the ladder diagrams are resummed to infinite order. The Brandow convention [76] is used. Wiggle lines represent anti-symmetrized two-electron integrals, summation over a, b, i, j is implied.

E_c^{MP2}. However, given the computational cost of self-consistent FMP2 calculations, neither straightforward perturbation expansion to third or fourth order, nor coupled-cluster-type resummations of the perturbation series are particularly attractive in the context of DFT. Thus, the question is whether one can find a minimal extension of E_c^{MP2} which just resolves the most obvious deficiencies of this functional, without introducing any additional computational effort?

The simplest class of diagrams allowing for resummation are the Epstein–Nesbet-type (EN) diagrams [74, 75], illustrated in Figure 7. If one restricts the resummation to the hole–hole diagrams explicitly shown, the resulting correlation functional reads [77]:

$$E_c^{\mathrm{HHEN}} = \frac{1}{4}\sum_{ijab}\frac{\Theta_i\Theta_j\bar{\Theta}_a\bar{\Theta}_b|(ij\|ab)-(ij\|ba)|^2}{\varepsilon_i+\varepsilon_j-\varepsilon_a-\varepsilon_b-(ij\|ij)+(ij\|ji)}. \quad (57)$$

Compared with a complete resummation of the EN series, this expression has the advantage that no additional matrix elements have to be evaluated: $(ij\|ij)$ and $(ij|ji)$ have to be calculated anyway (in the context of E_{H} and E_x). Moreover, $(ij\|ij)-(ij\|ji)\geq 0$, so that the hole–hole EN shift in the MP2 denominator is sign definite, thus enlarging the absolute value of the denominator.

E_c^{HHEN} as defined in Eq. (58) still suffers from its lacking invariance under unitary transformations in degenerate subspaces. For applications, it is therefore necessary to redefine E_c^{HHEN} as

$$E_c^{\mathrm{HHEN}} = \frac{1}{4}\sum_{ijab}\frac{\Theta_i\Theta_j\bar{\Theta}_a\bar{\Theta}_b|(ij\|ab)-(ij\|ba)|^2}{\varepsilon_i+\varepsilon_j-\varepsilon_a-\varepsilon_b-\overline{(ij\|ij)}+\overline{(ij\|ji)}}, \quad (58)$$

where $\overline{(ij\|ij)}$ implies averaging of $(ij\|ij)$ over degenerate subspaces. The correlation functional (58) will be called the hole–hole Epstein–Nesbet (HHEN) functional in the following.

In spite of the fact that E_c^{HHEN} includes more diagrammatic contributions than E_c^{MP2}, it is by no means clear a priori that this quite restricted resummation improves the final results (beyond the stabilization of critical systems). Applications are required to verify that E_c^{HHEN} represents some progress.

Results obtained with the combination of the exact E_x and E_c^{HHEN} (FHHEN) are included in Tables I, V, and VI as well as Figures 3 and 8. First, Table I demonstrates that the overestimation of atomic correlation energies by E_c^{MP2} is significantly reduced by the HHEN functional. More important, however, is the fact that E_c^{HHEN} no longer shows the variational instability observed for the MP2 expression in the case of the Be atom: Self-consistency is now easily attained, the HOMO–LUMO gap remains finite. The corresponding self-consistent correlation potential is displayed in Figure 8. The dramatic improvement over the pure MP2 potential (evaluated with x-only orbitals) is obvious. The same improvement is found when both functionals are evaluated with the exact KS orbitals, as shown in Figure 3. The variational stability of E_c^{HHEN} is reflected by the stability of the correlation potential during the self-consistent iteration: The converged potential is not much different from the potential obtained from x-only orbitals. This implies that, in practice, a perturbative calculation of v_c on the basis

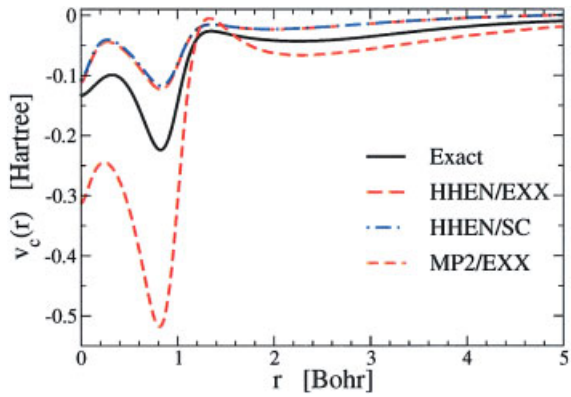

FIGURE 8. HHEN correlation potential for Be. Self-consistent potential (HHEN/SC) versus perturbative result obtained from the x-only density (HHEN/EXX). For comparison, the exact v_c and the MP2 potential resulting from the x-only density are plotted. [Color figure can be viewed in the online issue, which is available at www.interscience.wiley.com.]

of x-only results will be sufficient to provide a much improved KS potential.

In view of Figure 8, it is no surprise that E_c^{HHEN} also improves self-consistent total energies and IPs. Table V demonstrates that the average error in ground-state energies produced by E_c^{HHEN} is comparable to that of the BLYP functional. Moreover, E_c^{HHEN} is the first functional, which gives more accurate HOMO energies than x-only calculations (see Table VI). In other words: E_c^{HHEN} is the first functional for which the inclusion of the correlation potential in self-consistent KS calculations does not worsen the final results.

5. Concluding Remarks

The orbital-dependent approach opens a route for the construction of fully nonlocal, first-principles xc-functionals. By now, application of the simplest such functional, the exact exchange, is well established both in the case of molecular systems [19, 20, 24] and for solids [36–40, 42], with a number of efficient implementations being available [78–82]. As it is self-interaction free, the exact exchange allows us to deal with atomic negative ions [24, 33], improves bandgaps [38, 42], and provides an improved starting point for excited-state calculations based on the TDDFT or GW methods [83–86].

The development of first-priniciples orbital-dependent correlation functionals turns out to be a much greater challenge and is still in its early stage. It is obvious that the second-order perturbative functional studied in this contribution can only serve as a starting point. Nevertheless, this functional demonstrates the scientific potential of implicit correlation functionals: (i) it correctly accounts for the dispersion interaction; and (ii) it leads to realistic atomic correlation potentials, reproducing both the correct asymptotic behavior and the correct shell structure. The variational instability of this functional and its drastic overestimation of all correlation effects, on the other hand, suggest that straightforward perturbation theory is not the way to go. Partial resummation of the perturbation series is required, the most appropriate scheme depending on the system to be addressed, as well as on computational limitations. By incorporating the technically simplest class of higher-order contributions, the hole–hole Epstein–Nesbet diagrams, one obtains a functional that is variationally stable for all neutral atoms as well as singly and doubly ionized atoms considered so far. In addition, this functional yields much more accurate results than the second-order expression: The accuracy of the resulting ground state energies is comparable to that of state-of-the-art GGA functionals, and, even more important, the resulting correlation potential appears to be first potential whose inclusion in self-consistent calculations is preferable to the complete neglect of v_c.

ACKNOWLEDGMENTS

The calculations for this work have been performed on the computer cluster of the Center for Scientific Computing at J. W. Goethe-Universität Frankfurt.

References

1. Hohenberg, P.; Kohn, W. Phys Rev B 1964, 136, 864.
2. Kohn, W.; Sham, L. J. Phys Rev A 1965, 140, 1133.
3. Parr, R. G.; Yang, W. Density-Functional Theory of Atoms and Molecules; Oxford University Press: New York, 1989.
4. Dreizler, R. M.; Gross, E. K. U. Density Functional Theory; Springer: Berlin, 1990.
5. Fiolhais, C.; Nogeira, F.; Marques, M., Eds. Density Functional Theory; Lecture Notes in Physics; Springer: Berlin, 2003; Vol. 620.
6. Becke, A. D. Phys Rev A 1988, 38, 3098.
7. Lee, C.; Yang, W.; Parr, R. G. Phys Rev B 1988, 37, 785.
8. Perdew, J. P.; Burke, K.; Ernzerhof, M. Phys Rev Lett 1996, 77, 3865.
9. Shore, H. B.; Rose, J. H.; Zaremba, E. Phys Rev B 1977, 15, 2858.
10. Weimer, M.; Sala, F. D.; Görling, A. Chem Phys Lett 2003, 372, 538.
11. Filippi, C.; Singh, D. J.; Umrigar, C. J. Phys Rev B 1994, 50, 14947.
12. Barone, V.; Adamo, C.; Lelj, F. J Chem Phys 1995, 102, 364.
13. Leung, T. C.; Chan, C. T.; Harmon, B. N. Phys Rev B 1991, 44, 2923.
14. Dufek, P.; Blaha, P.; Schwarz, K. Phys Rev B 1994, 50, 7279.
15. Sahni, V.; Gruenebaum, J.; Perdew, J. P. Phys Rev B 1982, 26, 4371.
16. Langreth, D. C.; Mehl, M. J. Phys Rev B 1983, 28, 1809.
17. Krieger, J. B.; Li, Y.; Iafrate, G. J. Phys Rev A 1992, 45, 101.
18. Engel, E.; Vosko, S. H. Phys Rev A 1993, 47, 2800.
19. Görling, A. Phys Rev Lett 1999, 83, 5459.
20. Ivanov, S.; Hirata, S.; Bartlett, R. J. Phys Rev Lett 1999, 83, 5455.
21. Engel, E.; Höck, A.; Dreizler, R. M. Phys Rev A 2000, 61, 032502.
22. Engel, E.; Höck, A.; Dreizler, R. M. Phys Rev A 2000, 62, 042502.

23. Kim, Y.-H.; Städele, M.; Martin, R. M. Phys Rev A 1999, 60, 3633.
24. Engel, E.; Dreizler, R. M. J Comput Chem 1999, 20, 31.
25. Perdew, J. P.; Zunger, A. Phys Rev B 1981, 23, 5048.
26. Colle, R.; Salvetti, O. Theor Chim Acta (Berl) 1975, 37, 329.
27. Grabo, T.; Gross, E. K. U. Chem Phys Lett 1995, 240, 141.
28. Harris, J.; Jones, R. O. J Phys F 1974, 4, 1170.
29. Sham, L. J. Phys Rev B 1985, 32, 3876.
30. Görling, A.; Levy, M. Phys Rev A 1994, 50, 196.
31. Engel, E.; Facco Bonetti, A.; Keller, S.; Andrejkovics, I.; Dreizler, R. M. Phys Rev A 1998, 58, 964.
32. Kotani, T. J Phys: Condens Matter 1998, 10, 9241.
33. Li, Y.; Krieger, J. B.; Iafrate, G. J. Chem Phys Lett 1992, 191, 38.
34. Talman, J. D.; Shadwick, W. F. Phys Rev A 1976, 14, 36.
35. Engel, E.; Chevary, J. A.; Macdonald, L. D.; Vosko, S. H. Z Phys D 1992, 23, 7.
36. Kotani, T. Phys Rev B 1994, 50, 14816.
37. Kotani, T. Phys Rev Lett 1995, 74, 2989.
38. Kotani, T.; Akai, H. Phys Rev B 1996, 54, 16502.
39. Bylander, D. M.; Kleinman, L. Phys Rev Lett 1995, 74, 3660.
40. Bylander, D. M.; Kleinman, L. Phys Rev B 1995, 52, 14566.
41. Bylander, D. M.; Kleinman, L. Phys Rev B 1997, 55, 9432.
42. Städele, M.; Majewski, J. A.; Vogl, P.; Görling, A. Phys Rev Lett 1997, 79, 2089.
43. Sharp, R. T.; Horton, G. K. Phys Rev 1953, 90, 317.
44. Sham, L. J.; Schlüter, M. Phys Rev Lett 1983, 51, 1888.
45. Casida, M. E. Phys Rev A 1995, 51, 2505.
46. Engel, E. In Density Functional Theory; In Lecture Notes in Physics; Fiolhais, C.; Nogeira, F.; Marques, M., Eds.; Springer: Berlin, 2003; Vol 620; p 56.
47. Negele, J. W.; Orland, H. Quantum Many-Particle Systems; Addison-Wesley: Redwood City, CA, 1988.
48. Møller, C.; Plesset, M. S. Phys Rev 1934, 46, 618.
49. Chakravorty, S. J.; Gwaltney, S. R.; Davidson, E. R.; Parpia, F. A.; Fischer, C. F. Phys Rev A 1993, 47, 3649.
50. Vosko, S. H.; Wilk, L.; Nusair, M. Can J Phys 1980, 58, 1200.
51. Umrigar, C. J.; Gonze, X. Phys Rev A 1994, 50, 3827.
52. Tajti, A.; Szalay, P. G.; Császár, A. G.; Kallay, M.; Gauss, J.; Valeev, E. F.; Flowers, B. A.; Vásquez, J.; Stanton, J. F. J Chem Phys 2004, 121, 11599.
53. Huber, K. P.; Herzberg, G. L. Molecular Spectra and Molecular Structure. IV. Constants of Diatomic Molecules; Van Nostrand Reinhold: New York, 1979.
54. Lein, M.; Dobson, J. F.; Gross, E. K. U. J Comput Chem 1999, 20, 12.
55. Kumar, A.; Meath, W. J Mol Phys 1985, 54, 823.
56. Tang, K. T.; Norbeck, J. M.; Certain, P. R. J Chem Phys 1976, 64, 3063.
57. Silver, D. M. Phys Rev A 1980, 21, 1106.
58. Aziz, R. A.; Slaman, M. J. J Chem Phys 1991, 94, 8047.
59. Luo, F.; McBane, G.; Kim, G.; Giese, C. F.; Gentry, W. R. J Chem Phys 1993, 98, 3564.
60. Kelly, H. P. Phys Rev 1963, 131, 684.
61. Engel, E.; Jiang, H.; Bonetti, A. F. Phys Rev A 2005, 72, 052503.
62. Rose, M. E. Elementary Theory of Angular Momentum; Wiley: New York, 1957.
63. Morse, P. M.; Feshbach, H. Methods of Theoretical Physics; McGraw-Hill: New York, 1953.
64. Facco Bonetti, A.; Engel, E.; Schmid, R. N.; Dreizler, R. M. Phys Rev Lett 2001, 86, 2241.
65. Facco Bonetti, A.; Engel, E.; Schmid, R. N.; Dreizler, R. M. Phys Rev Lett 2003, 90, 219302.
66. Jiang, H.; Engel, E. J Chem Phys 2005, 123, 224102.
67. Grabowski, I.; Hirata, S.; Ivanov, S.; Bartlett, R. J. J Chem Phys 2002, 116, 4415.
68. Mori-Sanchez, P.; Wu, Q.; Yang, W. J Chem Phys 2005, 123, 062204.
69. Bartlett, R. J.; Grabowski, I.; Hirata, S.; Ivanov, S. J Chem Phys 2005, 123, 062205.
70. Chen, J.; Stott, M. J. Phys Lett A 1993, 176, 101.
71. Engel, E.; Vosko, S. H. Phys Rev B 1993, 47, 13164.
72. Chen, J.; Krieger, J. B.; Esquivel, R. O.; Stott, M. J.; Iafrate, G. J. Phys Rev A 1996, 54, 1910.
73. Almbladh, C.-O.; von Barth, U. Phys Rev B 1985, 31, 3231.
74. Wilson, S. Electron Correlation in Molecules; Clarendon Press: Oxford, 1984.
75. Szabo, A.; Ostlund, N. S. Modern Quantum Chemistry; Dover: New York, 1989.
76. Brandow, B. H. Rev Mod Phys 1967, 39, 771.
77. Jiang, H.; Engel, E. J Chem Phys 2006 (submitted).
78. Krieger, J. B.; Li, Y.; Iafrate, G. J. Phys Lett A 1990, 146, 256.
79. Engel, E.; Höck, A.; Schmid, R. N.; Dreizler, R. M.; Chetty, N. Phys Rev B 2001, 64, 125111.
80. Kümmel, S.; Perdew, J. P. Phys Rev Lett 2003, 90, 043004.
81. Sala, F. D.; Görling, A. J Chem Phys 2001, 115, 5718.
82. Yang, W.; Wu, Q. Phys Rev Lett 2002, 89, 143002.
83. Sala, F. D.; Görling, A. Int J Quantum Chem 2003, 91, 131.
84. Aulbur, W. G.; Städele, M.; Görling, A. Phys Rev B 2000, 62, 7121.
85. Fleszar, A. Phys Rev B 2001, 64, 245204.
86. Rinke, P.; Qteish, A.; Neugebauer, J.; Freysoldt, C.; Scheffer, M. New J Phys 2005, 7, 126.